Nonergodic Measurements of Qubit Frequency Noise

Filip Wudarski,[1] Yaxing Zhang,[2] and M. I. Dykman[3]

[1]*USRA Research Institute for Advanced Computer Science (RIACS), Mountain View, California 94043, USA*
[2]*Google Quantum AI, Santa Barbara, California 93111, USA*
[3]*Department of Physics and Astronomy, Michigan State University, East Lansing, Michigan 48824, USA*

Slow fluctuations of a qubit frequency are one of the major problems faced by quantum computers. To understand their origin it is necessary to go beyond the analysis of their spectra. We show that characteristic features of the fluctuations can be revealed using comparatively short sequences of periodically repeated Ramsey measurements, with the sequence duration smaller than needed for the noise to approach the ergodic limit. The outcomes distribution and its dependence on the sequence duration are sensitive to the nature of the noise. The time needed for quantum measurements to display quasiergodic behavior can strongly depend on the measurement parameters.

Introduction.—Because of the probabilistic nature of quantum measurements, many currently implemented quantum algorithms rely on repeatedly running a quantum computer. It is important that the qubit parameters remain essentially the same between the runs. This imposes a constraint on comparatively slow fluctuations of the qubit parameters, in particular qubit frequencies, and on developing means of revealing and characterizing such fluctuations.

Slow qubit frequency fluctuations have been a subject of intense studies [1–25]. Of primary interest has been their spectrum, although their statistics has also attracted interest [26–36]. This statistics may help to reveal the source of the underlying noise. In particular, fluctuations from the coupling to a few two-level systems (TLSs) should be non-Gaussian [27,32,37–43]. They are particularly important for solid state-based qubits, including those based on Josephson junctions and spin and charge states in semiconductors. Fluctuation statistics has been often described in terms of higher-order time correlators. Most work thus far has been done on fluctuations with the correlation time smaller than the qubit decay time.

Here we show that important information about qubit frequency fluctuations can be extracted from what we call nonergodic measurements. The idea is to perform M successive qubit measurements over time longer than the qubit decay time but shorter than the noise correlation time. The measurement outcomes are determined by the instantaneous state of the noise source, for example, by the instantaneous TLSs' states. They vary from one series of M measurements to another. Thus the outcome distribution reflects the distribution of the noise source over its states. It provides information that is washed out in the ensemble averaging inherent to ergodic measurements.

Closely related is the question of how long should a quantum measurement sequence be in order to reach the ergodic limit. Does the measurement duration depend on the type and parameters of the measurement, not only the noise source properties, and if so, on which parameters?

A convenient and frequently used method of performing successive measurements is to repeat them periodically. In this case the duration of data acquisition of M measurements is $\propto M$. For the measurements to be nonergodic it should suffice for this duration to be smaller than the noise correlation time. This imposes a limitation on M from above. The limitation on M from below is imposed by the uncertainty that comes from the quantum nature of the measurements.

We consider a periodic sequence of Ramsey measurements sketched in Fig. 1. At the beginning of a measurement, the qubit, initially in the ground state $|0\rangle$, is rotated about the y axis of the Bloch sphere by $\pi/2$, which brings it to the state $(|0\rangle + |1\rangle)/\sqrt{2}$. After time t_R the rotation is repeated and is followed by a projective measurement of finding the qubit in state $|1\rangle$. The qubit is then reset to $|0\rangle$, cf. [44]. In our scheme the measurements are repeated $M \gg 1$ times, with period t_{cyc}.
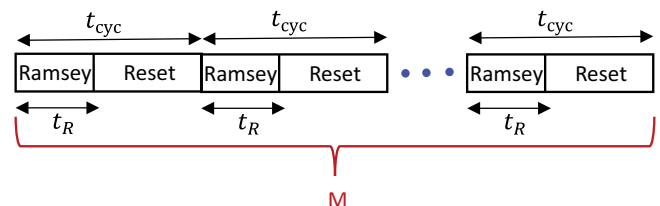

FIG. 1. Schematics of M Ramsey measurements. In each measurement the qubit phase is accumulated over time t_R. The measurements give the probability p to find the qubit in state $|1\rangle$. After a measurement the qubit is reset to state $|0\rangle$. The measurements are repeated with period t_{cyc}.

The outcome of a kth Ramsey measurement x_k is 0 or 1. The probability p to find $x_k = 1$ is determined by the qubit phase accumulated over time t_R. This phase comes from the detuning of the qubit frequency from the frequency of the reference drive and from the noise-induced qubit frequency fluctuations $\delta\omega_q(t)$. The detuning is controllable, and we will use ϕ_R to indicate the phase that comes from it. The Hamiltonian H_{fl} that describes frequency fluctuations and the phase θ_k accumulated in the kth measurement due to these fluctuations have the form

$$H_{fl} = -\frac{1}{2}\delta\omega_q(t)\sigma_z, \quad \theta_k = \int_{kt_{cyc}}^{kt_{cyc}+t_R}\delta\omega_q(t)dt \quad (1)$$

(we set $\hbar = 1$); we associate the Pauli operators $\sigma_{x,y,z}$ with the operators acting on the qubit states. We are interested in slow frequency fluctuations. The correlation time of $\delta\omega_q(t)$ is $\gtrsim t_{cyc}$.

In terms of the phases θ and ϕ_R, the probability to have $x_k = 1$ is [45]

$$p(\theta) = \frac{1}{2}\left[1 + e^{-t_R/T_2}\cos(\phi_R + \theta)\right], \quad (2)$$

where T_2^{-1} is the qubit decoherence rate due to fast processes leading to decay and dephasing. In the absence of qubit frequency noise $\theta = 0$ for all M measurements and the distribution of the measurement outcomes is a binomial distribution [46]. Because of the frequency noise, the phase θ in Eq. (2) becomes random, and thus the probability $p(\theta)$ also becomes random. The outcomes distribution is determined by the distribution of the values of θ. The sensitivity of $p(\theta)$ to θ is reduced by errors in the Ramsey gates, the preparation of the state $|0\rangle$, and the readout errors [47]. However, these errors are small. Moreover, they do not change the qualitative features of nonergodic measurements.

The randomness of the phase is captured by the probability $\rho(m|M)$ to have $x_k = 1$ as a measurement outcome m times in M measurements, $\rho(m|M) = \text{Prob}(\sum_{k=1}^M x_k = m)$. We consider $\rho(m|M)$ for periodically repeated measurements, see Fig. 1. If the frequency noise has correlation time small compared to the period t_{cyc}, the phases θ_k in successive measurements are uncorrelated. Then $\rho(m|M)$ is still given by a binomial distribution,

$$\rho_{binom}(m|M) = \binom{M}{m}r_1^m(1-r_1)^{M-m}, \quad (3)$$

where $r_1 \equiv \langle x_k \rangle = \langle p(\theta)\rangle_\theta$; here $\langle\ldots\rangle_\theta$ indicates averaging over realizations of θ. For large M this distribution is close to a Gaussian peak centered at r_1.

We are interested in the opposite case of slow frequency noise. Here the distribution $\rho(m|M)$ can strongly deviate

from the binomial distribution. The deviation becomes pronounced and characteristic of the noise if Mt_{cyc} is comparable or smaller than the noise correlation time while M is still large.

The effect is particularly clear in the *static limit*, where the noise does not change over time Mt_{cyc}, i.e., the phase θ remains constant during M measurements. Even though θ is constant, its value $\theta = \theta(\ell)$ is random, it varies from one series of M measurements to another. Here ℓ enumerates the possible discrete values of θ, which are determined, for example, by the states of the TLSs, and we assume that noise correlations decay between successive series. The probability $P[\theta(\ell)]$ to have a given $\theta(\ell)$ is determined by the noise statistics. The distribution of the outcomes $\rho(m|M)$ is obtained by averaging the results of multiple repeated series of M measurements. Extending the familiar arguments that lead to Eq. (3), we find

$$\rho(m|M) = \binom{M}{m}\sum_\ell P[\theta(\ell)]p^m[\theta(\ell)]$$
$$\times \{1 - p[\theta(\ell)]\}^{M-m}. \quad (4)$$

The distribution (4) directly reflects the distribution of the noise over its states. In particular, if the values of $\theta(\ell)$ are discrete and well separated (see an example below), $\rho(m|M)$ has a characteristic fine structure with peaks located at $m \approx Mp[\theta(\ell)]$ for $M \gg 1$; the peak heights are determined by $P[\theta(\ell)]$.

An important example of slow frequency noise is the noise that results from dispersive coupling to a set of slowly switching TLSs,

$$\delta\hat{\omega}_q(t) = \sum_n V^{(n)}(\hat{\tau}_z^{(n)} - \langle\hat{\tau}_z^{(n)}\rangle). \quad (5)$$

Here $n = 1, \ldots, N_{TLS}$ enumerates the TLSs, $\hat{\tau}_z^{(n)}$ is the Pauli operator of the nth TLS, $\langle\hat{\tau}_z^{(n)}\rangle$ is its average value, and $V^{(n)}$ is the coupling parameter; the states of the nth TLS are $|0\rangle^{(n)}$ and $|1\rangle^{(n)}$, and $\hat{\tau}_z^{(n)}|i\rangle^{(n)} = (-1)^i|i\rangle^{(n)}$ with $i = 0, 1$. We assume that the TLSs do not interact with each other. Their dynamics is described by the balance equations for the state populations. The only parameters are the rates $W_{ij}^{(n)}$ of $|i\rangle^{(n)} \to |j\rangle^{(n)}$ transitions, where $i, j = 0, 1$ [48].

The rates $W_{ij}^{(n)}$ give the stationary occupations of the TLSs states $w_{0,1}^{(n)}$, with $w_0^{(n)} = W_{10}^{(n)}/W^{(n)}$, $w_1^{(n)} = 1 - w_0^{(n)}$. Parameter $W^{(n)} = W_{01}^{(n)} + W_{10}^{(n)}$ is the TLS relaxation rate. The value of $\min W^{(n)}$ gives the reciprocal correlation time of the noise from the TLSs. We disregard the effect of the qubit on the TLSs dynamics, including measurements and resets, assuming that the TLSs decoherence rates are much larger than $V^{(n)}$. This is a good approximation for low-frequency TLSs coupled to solid-state based qubits.

In the static-limit approximation, the TLSs remain in the initially occupied states $|0\rangle^{(n)}$ or $|1\rangle^{(n)}$ during all M measurements. Then, from Eq. (5), the phase that the qubit accumulates during a measurement (before subtracting the average accumulated phase) is $\theta(\{j_n\}) = \sum_n (-1)^{j_n} V^{(n)} t_R$. Here $j_n = 0$ if the occupied TLS state is $|0\rangle^{(n)}$ and $j_n = 1$ if the occupied state is $|1\rangle^{(n)}$. The probability to have a given $\theta(\{j_n\})$ is determined by the stationary state occupations, $P[\theta(\{j_n\})] = \prod_n w_{j_n}^{(n)}$.

For the TLSs' induced noise, ℓ in Eq. (4) enumerates various combinations $\{j_n\}$. With the increasing coupling $V^{(n)}$, the separation of the values of $\theta(\{j_n\})$ increases, helping to observe the fine structure of $\rho(m|M)$.

The expression for $\rho(m|M)$ simplifies in the important case where the TLSs are symmetric, $w_0^{(n)} = w_1^{(n)} = 1/2$, and all coupling parameters are the same, $V^{(n)} = V$, cf. [2,10]. In this case $\theta(\{j_n\})$ takes on values $\theta_{\text{sym}}(\ell) = V t_R (2\ell - N_{\text{TLS}})$ with $0 \le \ell \le N_{\text{TLS}}$, and

$$\rho(m|M) = 2^{-N_{\text{TLS}}} \binom{M}{m} \sum_\ell \binom{N_{\text{TLS}}}{\ell} p^m [\theta_{\text{sym}}(\ell)]$$
$$\times \{1 - p[\theta_{\text{sym}}(\ell)]\}^{M-m}. \quad (6)$$

The phases $\theta_{\text{sym}}(\ell)$ are determined by the coupling constant V multiplied by the difference of the number of TLSs in the states $|0\rangle$ and $|1\rangle$, so that $\theta_{\text{sym}}(\ell)$ may be significantly larger than for a single TLS [47].

The probability $\rho(m|M)$ of having "1" m times in M measurements has a characteristic form also in the case of Gaussian frequency noise if the noise is slow, so that $\delta\omega_q(t)$ does not change over time $M t_{\text{cyc}}$. An important example of slow noise is $1/f$ noise. In the static limit

$\rho(m|M)$ is described by an extension of Eq. (4), which takes into account that θ takes on continuous values. Respectively, one has to change in Eq. (4) from the sum over ℓ to the integral over $\theta(\ell)$, with $P[\theta(\ell)]$ becoming the probability density. For Gaussian noise $P[\theta(\ell)] = (2\pi f_0)^{-1/2} \exp[-\theta^2(\ell)/2f_0]$, where $f_0 = \langle \delta\omega_q^2 \rangle t_R^2$ (we assume that $\langle \delta\omega_q \rangle = 0$). The distribution $\rho(m|M)$ does not have fine structure; it depends only on the noise intensity in the static limit.

The opposite of the static limit is the ergodic limit, where $M t_{\text{cyc}}$ is much larger than the noise correlation time and the noise has time to explore all states during the measurements. In this limit $\rho(m|M)$ as a function of m/M has a narrow peak at $r_1 = \langle m/M \rangle \equiv \sum_m (m/M) \rho(m|M)$, with $\langle [(m/M) - r_1]^n \rangle \propto M^{-n/2}$ for even n.

Simulations.—We performed numerical simulations to explore the transition from the static to the ergodic limit and the features of $\rho(m|M)$ for slow noise. Here we present the results for $t_{\text{cyc}} = 3 t_R$. This ratio can be easily implemented in experiment. For example, for transmons a limit imposed by decay and fast dephasing is $t_R \lesssim 0.3$ ms, whereas the gate duration is $\lesssim 25$ ns and the reset time can be $\lesssim 0.5$ μs [49–51]. Choosing t_{cyc} of order of a few t_R allows applying the results to the noise in the kilohertz range, which plays an important role in transmons. The simulations were repeated at least 10^5 times. In Fig. 2 we show $\rho(m|M)$ for the noise from symmetric TLSs, $W_{01}^{(n)} = W_{10}^{(n)} = W^{(n)}/2$ (see [47] for other t_{cyc}/t_R and for the results on asymmetric TLSs).

Figure 2 shows evolution of $\rho(m|M)$ with the varying measurements number M. It is very different for different numbers of TLSs and the measurement parameter ϕ_R. The figure refers to a relatively weak qubit-TLS coupling. Panel (a) refers to a single TLS. Here, in the static limit
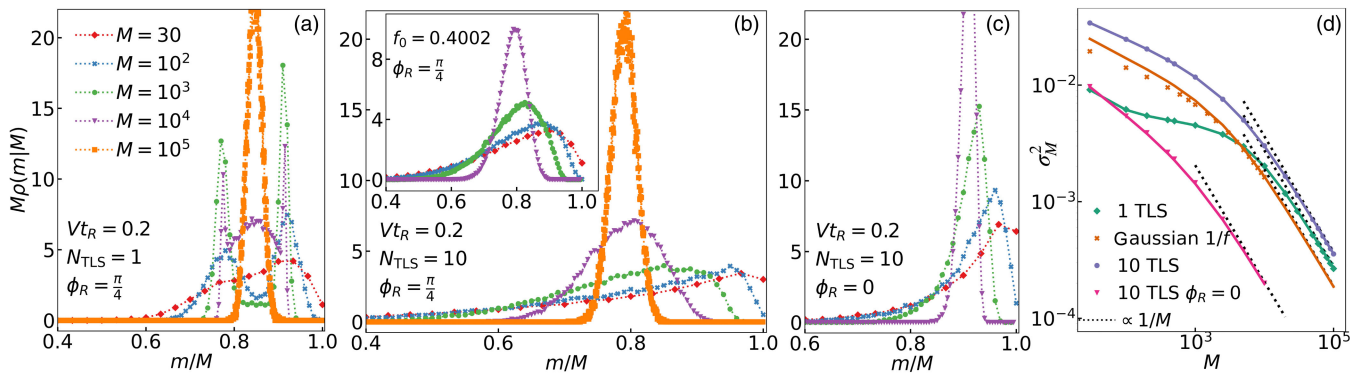

FIG. 2. Transition from nonergodic to ergodic behavior with the increasing number of measurements. Red diamonds, blue crosses, green dots, purple triangles, and orange squares in panels (a)–(c) show $\rho(m|M)$ for $M = 30, 10^2, 10^3, 10^4$, and 10^5, respectively. The scaled parameter of the dispersive qubit-to-TLS coupling is $V t_R = 0.2$. The control parameter ϕ_R is $\pi/4$ in (a) and (b). (a) Coupling to a single symmetric TLS with the scaled switching rate $W t_R = 1.2 \times 10^{-4}$. (b) Coupling to 10 symmetric TLSs with the switching rates $W^{(n)} t_R = \exp(-3n/4)$, $n = 3, 4, \ldots, 12$. The inset shows the results for Gaussian $1/f$-type noise described in the text, $f_0 = \langle \delta\omega_q^2 \rangle t_R^2$. (c) Coupling to the same 10 TLSs as in panel (b), but for $\phi_R = 0$. (d) Variance of $\rho(m|M)$ for the data in panels (a)–(c); solid lines show the theory; data points show the results of the simulations; dashed lines show the ergodic limit.

$\rho(m|M)$ is double peaked, with the peaks at $m/M \approx 0.92$ and 0.78, from Eq. (6). Such peaks are seen for $M = 10^2$, 10^3, and 10^4, where MWt_{cyc} varies from 0.036 to 3.6, even though one might expect the system to be close to ergodic for $M = 10^4$. For $M = 30$ the fine structure is smeared, because M is not large enough to average out the uncertainty of quantum measurements, but $\rho(m|M)$ displays a significant and characteristic asymmetry. For $M = 10^5$, where $MWt_{\text{cyc}} = 36$, the distribution does approach the ergodic limit, with a single peak at $m/M \approx 0.85$ [47].

Figure 2(b) refers to 10 TLSs. Their scaled switching rates $W^{(n)}t_{\text{cyc}}$ form a geometric series, varying from ≈ 0.32 to $\approx 3.7 \times 10^{-4}$. The power spectrum of the noise $\delta\omega_q(t)$ is close to $1/f$ in a broad frequency range for such form of $W^{(n)}$ [47]. However, for the chosen $W^{(n)}t_{\text{cyc}}$ the static limit does not apply and the fine structure is not resolved. The asymmetry of $\rho(m|M)$ is profound. It gradually decreases with the increasing M. It is important that, for $\phi_R = \pi/4$, the distribution approaches the ergodic limit for $Mt_{\text{cyc}} \times (\min W^{(n)}) \gtrsim 30$, similar to the case of one TLS (the choice $\phi_R = \pi/4$ is explained in [47]).

For comparison, the inset in Fig. 2(b) shows the evolution of $\rho(m|M)$ for $1/f$-type Gaussian frequency noise $\delta\omega_q(t)$ with the power spectrum $S_q(\omega) = (2D/\pi) \int_{\omega_{\min}}^{\infty} dW/(W^2 + \omega^2)$. The cutoff frequency $\omega_{\min}$ is set equal to the minimal switching rate of the 10 TLSs in the main panel $\min(W^{(n)})$, and the intensity D is chosen so that, in the ergodic limit, $\rho(m|M)$ has a maximum for the same m/M as for the 10 TLSs.

The result of Fig. 2(c) is surprising. The data refers to the same 10 TLSs as in panel (b), except that the phase of the Ramsey measurement is set to $\phi_R = 0$. The change of ϕ_R does not affect the dynamics of the TLSs. However, for the same M values, the peak of $\rho(m|M)$ is much narrower than for $\phi_R = \pi/4$ and $\rho(m|M)$ approaches the ergodic limit for an order of magnitude smaller M.

A simple measure of closeness of $\rho(m|M)$ to the ergodic limit is the variance $\sigma_M^2 = \sum_m (m/M)^2 \rho(m|M) - r_1^2$, where $r_1 = \langle x_k \rangle$. It is expressed in terms of the pair correlator of x_k [47]. In the ergodic limit $\sigma_M^2 \propto M^{-1}$, but its value depends on the noise correlation. Figure 2(d) shows how σ_M^2 approaches the ergodic scaling [52]. For $\phi_R = \pi/4$ and the same correlation time of the noise from 1 or 10 TLSs and of Gaussian noise ($\sim 1/\min W^{(n)}$ and $\sim 1/\omega_{\min}$), σ_M^2 behaves similarly for large M. Yet, for the same 10 TLSs, but for $\phi_R = 0$ the variance approaches the ergodic limit much faster.

The fine structure of $\rho(m|M)$ is more pronounced for larger scaled coupling $|V|t_R$. For example, for one TLS the interpeak distance is $\approx \sin(Vt_R) \sin\phi_R$. It is important that the coupling parameter Vt_R can be changed in the experiment by varying t_R. The ratio between Mt_{cyc} and the noise correlation time can be changed, too, and not only

by varying M (which affects the statistics), but also by varying t_{cyc}. The fine structure is more pronounced for smaller t_{cyc} [47].

In a qualitative distinction from the power spectrum of the frequency noise, which has the same form for a symmetric and an asymmetric TLS, $\rho(m|M)$ sensitively depends on the TLS asymmetry. In particular, $\rho(m|M) = \rho(M - m|M)$ for $\phi_R = \pi/2$ for symmetric TLSs, whereas for asymmetric TLSs $\rho(m|M) \neq \rho(M - m|M)$; the fine structure is also better resolved for $\phi_R = \pi/2$ [47]. This shows that nonergodic measurements can be used to characterize the coupling to low-frequency TLSs, where the standard technique of tuning a qubit in resonance with a TLS does not apply.

The presence of a characteristic fine structure of $\rho(m|M)$ is an unambiguous indication of the noise coming from the coupling to slow TLSs. Observing it would be a long-sought direct proof of the nature of the low-frequency noise, which was early on associated with, but not directly proved to be caused by, TLSs [2]. For large N_{TLS} it becomes more complicated to characterize individual TLSs using $\rho(m|M)$ as the peaks of $\rho(m|M)$ start overlapping. However, for small $N_{\text{TLS}} \lesssim 5$ our simulations show that the number of peaks of the fine structure and their amplitudes and shapes still enable estimating the number and the parameters of slow TLSs.

For 10 TLSs, as seen in panel (b), the distribution is broad and strongly asymmetric. Both its shape and the position of the maximum sensitively depend on the coupling. We note the distinction from direct measurements of qubit frequency as a function of time [3,6,21], which is efficient for still much slower noise.

Nonergodic measurements are more revealing in terms of the mechanism of low-frequency noise than the ergodic ones [52], particularly where the fine structure is pronounced. In addition to t_R, t_{cyc}, and ϕ_R, they have M as an important control parameter. However, the two methods complement each other. Besides the TLSs, nonergodic measurements can be used to study other low-frequency noise sources, such as the noise from photons in a superconducting cavity and from nuclear spins in electron spin based qubits.

Discussion of ergodicity.—To reach ergodic limit, a system of 10 TLSs has to visit its 2^{10} states. The needed time is a property of the TLSs themselves. However, the results of the measurements can approach a quasiergodic limit, except for the far tail of the outcomes distribution, over a shorter time. This time depends on the correlation time of the fluctuations relevant for the measurement, but this correlation time is not obvious in advance. In our setup, the noise is "measured" by the qubit, and then the results are read through Ramsey measurements. As we show, an important parameter is the qubit-to-TLSs coupling, which we chose to be the same for all TLSs to avoid any bias. Unexpectedly, there is another important parameter, the phase ϕ_R.

The effect of ϕ_R on the convergence to the ergodic limit is not obvious in advance. It is seen already in the dependence on ϕ_R of the centered correlator $\tilde{r}_2(k)$ of the measurement outcomes. For weak coupling to slowly switching TLSs, $V^{(n)}t_R \ll 1$ and $W^{(n)}t_R \ll 1$, and for $|\phi_R| \ll 1$ this correlator is small. Moreover, it falls off with the increasing k much faster than for $\phi_R = \mathcal{O}(1)$ [47]. This indicates a reduced role of slow noise correlations for small ϕ_R. Respectively, the ergodic limit is reached much faster with the increasing M.

Conclusions.—We studied the distribution of the outcomes of periodically repeated Ramsey measurements with the sequence length Mt_{cyc} shorter than needed to approach the ergodic limit. Such distribution proves to provide an alternative, and sensitive, means of characterizing qubit frequency noise with a long correlation time. In contrast to bi- or trispectra, such distribution incorporates noise correlators of order $M \gg 1$. The analytical results and simulations show that, for non-Gaussian noise, in particular the noise from TLSs, the distribution can display a characteristic fine structure. Even where there is no fine structure, the form of the distribution and its evolution with the sequence length are noise specific.

The results show that the way the system approaches the ergodic limit with the increasing number of quantum measurements depends not only on the noise source but also on the character and parameters of the measurement. These parameters are not necessarily known in advance. Their effect can be strong and depends on the noise source. Measurement outcomes can practically approach the ergodic limit well before the noise source approaches this limit.

---

[1] Y. Nakamura, Yu. A. Pashkin, T. Yamamoto, and J. S. Tsai, Charge echo in a Cooper-pair box, Phys. Rev. Lett. **88**, 047901 (2002).

[2] G. Ithier, E. Collin, P. Joyez, P. J. Meeson, D. Vion, D. Esteve, F. Chiarello, A. Shnirman, Y. Makhlin, J. Schriefl, and G. Schön, Decoherence in a superconducting quantum bit circuit, Phys. Rev. B **72**, 134519 (2005).

[3] R. C. Bialczak, R. McDermott, M. Ansmann, M. Hofheinz, N. Katz, E. Lucero, M. Neeley, A. D. O'Connell, H. Wang, A. N. Cleland, and J. M. Martinis, $1/f$ flux noise in Josephson phase qubits, Phys. Rev. Lett. **99**, 187006 (2007).

[4] G. A. Álvarez and D. Suter, Measuring the spectrum of colored noise by dynamical decoupling, Phys. Rev. Lett. **107**, 230501 (2011).

[5] J. Bylander, S. Gustavsson, F. Yan, F. Yoshihara, K. Harrabi, G. Fitch, D. G. Cory, Y. Nakamura, J.-S. Tsai, and W. D. Oliver, Noise spectroscopy through dynamical decoupling with a superconducting flux qubit, Nat. Phys. **7**, 565 (2011).

[6] D. Sank, R. Barends, R. C. Bialczak, Y. Chen, J. Kelly, M. Lenander, E. Lucero, M. Mariantoni, A. Megrant, M. Neeley, P. J. J. O'Malley, A. Vainsencher, H. Wang, J. Wenner, T. C. White, T. Yamamoto, Y. Yin, A. N. Cleland, and J. M. Martinis, Flux noise probed with real time qubit tomography in a Josephson phase qubit, Phys. Rev. Lett. **109**, 067001 (2012).

[7] F. Yan, J. Bylander, S. Gustavsson, F. Yoshihara, K. Harrabi, D. G. Cory, T. P. Orlando, Y. Nakamura, J.-S. Tsai, and W. D. Oliver, Spectroscopy of low-frequency noise and its temperature dependence in a superconducting qubit, Phys. Rev. B **85**, 174521 (2012).

[8] K. C. Young and K. B. Whaley, Qubits as spectrometers of dephasing noise, Phys. Rev. A **86**, 012314 (2012).

[9] G. A. Paz-Silva and L. Viola, General transfer-function approach to noise filtering in open-loop quantum control, Phys. Rev. Lett. **113**, 250501 (2014).

[10] F. Yoshihara, Y. Nakamura, F. Yan, S. Gustavsson, J. Bylander, W. D. Oliver, and J.-S. Tsai, Flux qubit noise spectroscopy using Rabi oscillations under strong driving conditions, Phys. Rev. B **89**, 020503(R) (2014).

[11] M. Kim, H. J. Mamin, M. H. Sherwood, K. Ohno, D. D. Awschalom, and D. Rugar, Decoherence of near-surface nitrogen-vacancy centers due to electric field noise, Phys. Rev. Lett. **115**, 087602 (2015).

[12] M. Brownnutt, M. Kumph, P. Rabl, and R. Blatt, Ion-trap measurements of electric-field noise near surfaces, Rev. Mod. Phys. **87**, 1419 (2015).

[13] P. J. J. O'Malley *et al.*, Qubit metrology of ultralow phase noise using randomized benchmarking, Phys. Rev. Appl. **3**, 044009 (2015).

[14] F. Yan, S. Gustavsson, A. Kamal, J. Birenbaum, A. P. Sears, D. Hover, T. J. Gudmundsen, D. Rosenberg, G. Samach, S. Weber, J. L. Yoder, T. P. Orlando, J. Clarke, A. J. Kerman, and W. D. Oliver, The flux qubit revisited to enhance coherence and reproducibility, Nat. Commun. **7**, 1 (2016).

[15] B. A. Myers, A. Ariyaratne, and A. C. B. Jayich, Double-quantum spin-relaxation limits to coherence of near-surface nitrogen-vacancy centers, Phys. Rev. Lett. **118**, 197201 (2017).

[16] C. M. Quintana *et al.*, Observation of classical-quantum crossover of $1/f$ flux noise and its paramagnetic temperature dependence, Phys. Rev. Lett. **118**, 057702 (2017).

[17] G. A. Paz-Silva, L. M. Norris, and L. Viola, Multiqubit spectroscopy of Gaussian quantum noise, Phys. Rev. A **95**, 022121 (2017).

[18] C. Ferrie, C. Granade, G. Paz-Silva, and H. M. Wiseman, Bayesian quantum noise spectroscopy, New J. Phys. **20**, 123005 (2018).

[19] C. Noel, M. Berlin-Udi, C. Matthiesen, J. Yu, Y. Zhou, V. Lordi, and H. Häffner, Electric-field noise from thermally activated fluctuators in a surface ion trap, Phys. Rev. A **99**, 063427 (2019).

[20] U. von Lüpke, F. Beaudoin, L. M. Norris, Y. Sung, R. Winik, J. Y. Qiu, M. Kjaergaard, D. Kim, J. Yoder, S. Gustavsson, L. Viola, and W. D. Oliver, Two-qubit spectroscopy of spatiotemporally correlated quantum noise in superconducting qubits, PRX Quantum **1**, 010305 (2020).

[21] T. Proctor, M. Revelle, E. Nielsen, K. Rudinger, D. Lobser, P. Maunz, R. Blume-Kohout, and K. Young, Detecting and

tracking drift in quantum information processors, Nat. Commun. **11**, 5396 (2020).

[22] G. Wolfowicz, F. J. Heremans, C. P. Anderson, S. Kanai, H. Seo, A. Gali, G. Galli, and D. D. Awschalom, Qubit guidelines for solid-state spin defects, Nat. Rev. Mater. **6**, 906 (2021).

[23] Y.-X. Wang and A. A. Clerk, Intrinsic and induced quantum quenches for enhancing qubit-based quantum noise spectroscopy, Nat. Commun. **12**, 6528 (2021).

[24] G. Burkard, T. D. Ladd, A. Pan, J. M. Nichol, and J. R. Petta, Semiconductor spin qubits, Rev. Mod. Phys. **95**, 025003 (2023).

[25] S. Burgardt, S. B. Jäger, J. Feß, S. Hiebel, I. Schneider, and A. Widera, Measuring the environment of a Cs qubit with dynamical decoupling sequences, J. Phys. B **56**, 165501 (2023).

[26] F. Li, A. Saxena, D. Smith, and N. A. Sinitsyn, Higher-order spin noise statistics, New J. Phys. **15**, 113038 (2013).

[27] G. Ramon, Non-Gaussian signatures and collective effects in charge noise affecting a dynamically decoupled qubit, Phys. Rev. B **92**, 155422 (2015).

[28] L. M. Norris, G. A. Paz-Silva, and L. Viola, Qubit noise spectroscopy for non-Gaussian dephasing environments, Phys. Rev. Lett. **116**, 150503 (2016).

[29] N. A. Sinitsyn and Y. V. Pershin, The theory of spin noise spectroscopy: A review, Rep. Prog. Phys. **79**, 106501 (2016).

[30] P. Szańkowski, G. Ramon, J. Krzywda, D. Kwiatkowski, and L Cywiński, Environmental noise spectroscopy with qubits subjected to dynamical decoupling, J. Phys. Condens. Matter **29**, 333001 (2017).

[31] Y. Sung, F. Beaudoin, L. M. Norris, F. Yan, D. K. Kim, J. Y. Qiu, U. von Lüpke, J. L. Yoder, T. P. Orlando, S. Gustavsson, L. Viola, and W. D. Oliver, Non-Gaussian noise spectroscopy with a superconducting qubit sensor, Nat. Commun. **10**, 3715 (2019).

[32] G. Ramon, Trispectrum reconstruction of non-Gaussian noise, Phys. Rev. B **100**, 161302(R) (2019).

[33] J. J. Burnett, A. Bengtsson, M. Scigliuzzo, D. Niepce, M. Kudra, P. Delsing, and J. Bylander, Decoherence benchmarking of superconducting qubits, npj Quantum Inf. **5**, 1 (2019).

[34] F. Sakuldee and Ł. Cywiński, Relationship between subjecting the qubit to dynamical decoupling and to a sequence of projective measurements, Phys. Rev. A **101**, 042329 (2020).

[35] Y.-X. Wang and A. A. Clerk, Spectral characterization of non-Gaussian quantum noise: Keldysh approach and application to photon shot noise, Phys. Rev. Res. **2**, 033196 (2020).

[36] X. You, A. A. Clerk, and J. Koch, Positive- and negative-frequency noise from an ensemble of two-level fluctuators, Phys. Rev. Res. **3**, 013045 (2021).

[37] E. Paladino, L. Faoro, G. Falci, and R. Fazio, Decoherence and $1/f$ noise in Josephson qubits, Phys. Rev. Lett. **88**, 228304 (2002).

[38] Y. M. Galperin, B. L. Altshuler, and D. V. Shantsev, Low-frequency noise as a source of dephasing of a qubit, in *Fundamental Problems of Mesoscopic Physics*, edited by I. V. Lerner (Kluwer Academic Publishing, The Netherlands, 2004).

[39] L. Faoro and L. Viola, Dynamical suppression of $1/f$ noise processes in qubit systems, Phys. Rev. Lett. **92**, 117905 (2004).

[40] Y. M. Galperin, B. L. Altshuler, J. Bergli, and D. V. Shantsev, Non-Gaussian low-frequency noise as a source of qubit decoherence, Phys. Rev. Lett. **96**, 097009 (2006).

[41] E. Paladino, Y. M. Galperin, G. Falci, and B. L. Altshuler, $1/f$ noise: Implications for solid-state quantum information, Rev. Mod. Phys. **86**, 361 (2014).

[42] C. Müller, J. H. Cole, and J. Lisenfeld, Towards understanding two-level-systems in amorphous solids: Insights from quantum circuits, Rep. Prog. Phys. **82**, 124501 (2019).

[43] Z. Huang, X. You, U. Alyanak, A. Romanenko, A. Grassellino, and S. Zhu, High-order qubit dephasing at sweet spots by non-Gaussian fluctuators: Symmetry breaking and Floquet protection, Phys. Rev. Appl. **18**, L061001 (2022).

[44] T. Fink and H. Bluhm, Noise spectroscopy using correlations of single-shot qubit readout, Phys. Rev. Lett. **110**, 010403 (2013).

[45] M. A. Nielsen and I. L. Chuang, *Quantum Computation and Quantum Information: 10th Anniversary Edition* (Cambridge University Press, England, 2011).

[46] N. G. Van Kampen, *Stochastic Processes in Physics and Chemistry*, 3rd ed. (Elsevier, Amsterdam, 2007).

[47] See Supplemental Material at http://link.aps.org/supplemental/10.1103/PhysRevLett.131.230201 for more results on $\rho(m|M)$, including the fine structure, the effect of asymmetric TLSs, and the transition to the ergodic limit.

[48] P. W. Anderson, B. I. Halperin, and C. M. Varma, Anomalous low-temperature thermal properties of glasses and spin glasses, Philos. Mag. J. Theor. Exp. Appl. Phys. **25**, 1 (1972); W. A. Phillips, Tunneling states in amorphous solids, J. Low Temp. Phys. **7**, 351 (1972); W. A. Phillips, Two-level states in glasses, Rep. Prog. Phys. **50**, 1657 (1987).

[49] Google Quantum AI, Suppressing quantum errors by scaling a surface code logical qubit, Nature (London) **614**, 676 (2023).

[50] Y. Kim, A. Eddins, S. Anand, K. Wei, E. van den Berg, S. Rosenblatt, H. Nayfeh, Y. Wu, M. Zaletel, K. Temme, and A. Kandala, Evidence for the utility of quantum computing before fault tolerance, Nature (London) **618**, 1476 (2023).

[51] S. Krinner, N. Lacroix, A. Remm, A. D. Paolo, E. Genois, C. Leroux, C. Hellings, S. Lazar, F. Swiadek, J. Herrmann, G. J. Norris, C. K. Andersen, M. Müller, A. Blais, C. Eichler, and A. Wallraff, Realizing repeated quantum error correction in a distance-three surface code, Nature (London) **605**, 669 (2022).

[52] F. Wudarski, Y. Zhang, A. N. Korotkov, A. G. Petukhov, and M. I. Dykman, Characterizing low-frequency qubit noise, Phys. Rev. Appl. **19**, 064066 (2023).

Supplemental Material:
Nonergodic measurements of qubit frequency noise

Filip Wudarski

USRA Research Institute for Advanced Computer Science (RIACS), Mountain View, CA 94043, USA

Yaxing Zhang

Google Quantum AI, Santa Barbara, CA 93111 , USA

M. I. Dykman

Department of Physics and Astronomy, Michigan State University, East Lansing, MI 48824, USA

(Dated: November 1, 2023)

I. COUPLING TO ASYMMETRIC TWO-LEVEL SYSTEMS

Generally, the switching rates W_{ij} between the states $|i\rangle$ and $|j\rangle$ of a two-level system (TLS) are different. TLSs with $W_{ij} \neq W_{ji}$ are called asymmetric. Here we present the results that show the effect of the TLS asymmetry on the qubit frequency noise for slow TLSs, where the rates W_{ij} are much smaller than the reciprocal duration of the Ramsey measurement t_R^{-1}. We consider a sequence of measurements described in the main text, where Ramsey measurements are periodically repeated M times with period t_{cyc}, see Fig. 1 of the main text. Of interest is the probability $\rho(m|M)$ to have m out of M times "one" as an outcome of an individual Ramsey measurement.

A characteristic feature of the distribution $\rho(m|M)$ for the coupling to slow TLSs is the possibility to have a fine structure. The fine structure can be approximately described in the static limit, where we disregard switching between the TLS states during the time Mt_{cyc}.

A. Coupling to a single TLS

From Eq. (4) of the main text, in the static limit for the coupling to a single TLS with states $|0\rangle$ and $|1\rangle$,

$$\rho(m|M) = \binom{M}{m} \sum_{\ell=0,1} P[\theta(\ell)]p^m[\theta(\ell)]\{1 - p[\theta(\ell)]\}^{M-m},$$
$$\theta(\ell) = \theta_0(\ell) - \bar{\theta}, \quad \theta_0(\ell) = (-1)^\ell V t_R,$$
$$\bar{\theta} = \sum_\ell \theta_0(\ell)P[\theta(\ell)], \qquad P[(\theta(\ell)] = W_{1-\ell\,\ell}/W, \qquad \text{(S1)}$$

where $W = W_{01} + W_{10}$ is the relaxation rate of the TLS. As in the main text, in what follows we approximate the probability of having "one" as a measurement outcome by $p(\theta) = [1 + \cos(\theta + \phi_R)]/2$, i.e., we disregard decoherence due to fast processes (see also Sec. V below); $\theta = \int_0^{t_R} dt[\delta\omega_q(t) - \overline{\delta\omega_q(t)}]$ is the qubit phase accumulated during Ramsey measurement due to qubit frequency fluctuations $\delta\omega_q(t)$ (the overbar indicates ensemble averaging); ϕ_R is the controlled qubit phase, see the main text. Since the qubit frequency is determined

in the presence of noise, in the experiment it is defined so that $\overline{\delta\omega_q(t)} = 0$; therefore of significance is only the zero-mean part of θ as defined by the above expression.

For $M \gg 1$ the distribution (S1) has two peaks, which in the static limit would be located at $m/M = p[\theta(\ell)]$, be separated by $\approx \sin(Vt_R)\sin\phi_R$ (~ 0.14 for the parameters in the figure), and have intensities $\propto W_{1-\ell\,\ell}/W$ ($\ell = 0, 1$). Such peaks, albeit broadened due to the interstate switching, are seen in Fig. S1. The parameters are chosen so that the correlation times of the symmetric TLS W^{-1} and the asymmetric TLS $(W_{01} + W_{10})^{-1}$ are close to each other. The figure shows that the fine structure is different for a symmetric TLS [panels (a) and (c)] and an asymmetric TLS [panels (b) and (d)]. Different are both the relative heights of the peaks of $\rho(m|M)$, their widths, and how they evolve with the increasing M. In particular, in a certain range of M one can have $MW_{10}t_{\text{cyc}} > 1$ and $MW_{01}t_{\text{cyc}} < 1$, so that the TLS has time to switch from state $|1\rangle$ during the measurement sequence, but the probability to switch from state $|0\rangle$ is still relatively small. These features make it possible to characterize the TLS asymmetry, which may not be done even if the power spectrum of the qubit frequency is available.

The fine structure of $\rho(m|M)$ is more distinct when the correlation time of the noise $\delta\omega_q(t)$ exceeds the total duration of the measurement Mt_{cyc}, which suggests using shorter Mt_{cyc} to reveal it. However one still needs large M to suppress the inherent uncertainty of quantum measurements. A compromise can be reached by reducing the intervals t_{cyc} between successive Ramsey measurements, as seen from the data in Fig. S1 for different t_{cyc}. The transition to the ergodic limit occurs for smaller M when t_{cyc} is increased, as seen from panels (a) and (c). Interestingly, the merging of the peaks as the system moves toward the ergodic limit with the increasing M leads to $\rho(m|M)$ having 3 rather than 2 peaks, as seen in panels (a) and (c) for $M = 10^4$.

The fine structure of $\rho(m|M)$ becomes more visible if the coupling is increased, as seen in Fig. S2. For a symmetric TLS and $M = 10^2$, for $Vt_R \gtrsim 0.5$ the positions of the peaks are approaching the static-limit values, as seen in panels (a) and (c). For an asymmetric TLS the peaks are overlapping stronger, and therefore the maxima of
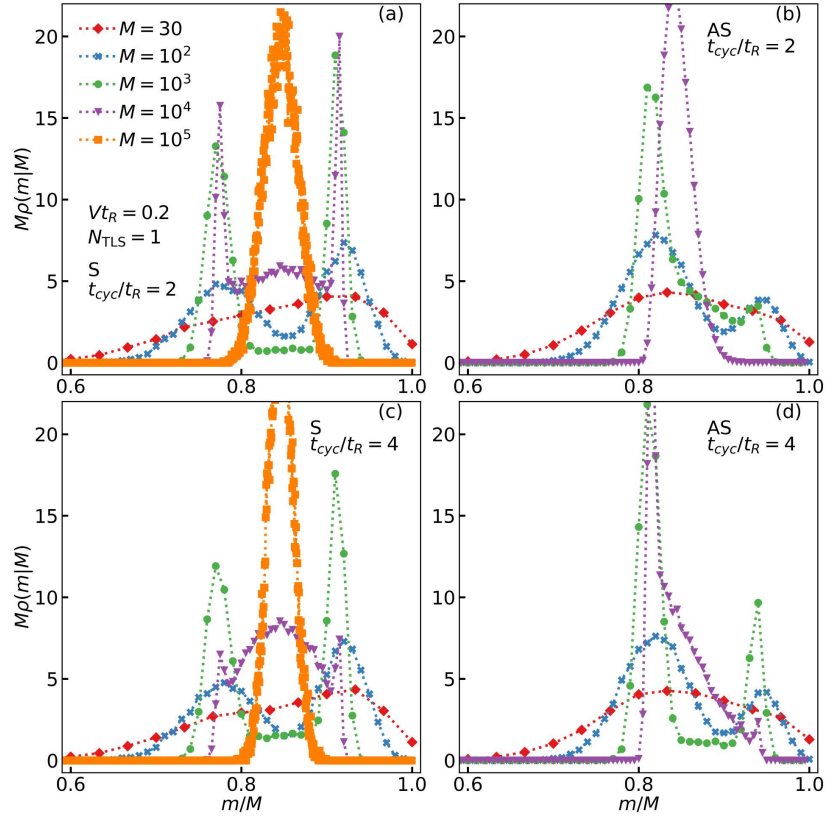
FIG. S1. Evolution of the probability distribution $\rho(m|M)$ with the varying number of measurements M for coupling to a single TLS. The letters S and AS indicate that the plots refer to a symmetric or an asymmetric TLS, respectively. The measurement phase is $\phi_R = \pi/4$. The number of Ramsey measurements in a sequence M and the scaled coupling parameter are indicated in the legend. For the symmetric TLS $Wt_R = 1.2 \times 10^{-4}$, whereas for the asymmetric TLS the scaled switching rates are $W_{10}t_R = 0.000075$ and $W_{01}t_R = 0.000025$. Panels (a) and (b) refer to the Ramsey measurements repeated with period $t_{\text{cyc}} = 2t_R$ and in panels (c) and (d) $t_{\text{cyc}} = 4t_R$. For the asymmetric TLS we do not show results for $M = 10^5$ to avoid a strong overlap with the data for smaller M.

$\rho(m|M)$ are shifted from the static-limit positions. More-over, it is seen even more clearly than in Fig. S1 that the areas of the peaks are different for an asymmetric TLS, since the stationary populations of the states responsible for the peaks are different.

B. Fine structure of the distribution for the coupling to multiple TLSs

As indicated in the main text, fine structure of $\rho(m|M)$ can become more pronounced for several TLSs than for one TLS, provided their switching rates are small. Fig-ure S3 illustrates this effect for the coupling to five TLSs. The system is the five slower-switching out of 10 TLSs studied in the main text, see Fig. 2 of the main text. For symmetric TLSs, in the static limit the qubit phase θ can take on 6 values, $\pm Vt_R, \pm 3Vt_R$, and $\pm 5Vt_R$. However, the static-limit theory lines in Fig. S3 (a) and (c) show 5 or 4 peaks, depending on the value of Vt_R. This is because, for the chosen $\phi_R = \pi/4$, some peaks appear to be too small to be resolved.

The value of $\phi_R = \pi/4$ is, in some sense, "generic". The measurement outcomes could be expected to be more sensitive to noise for $\phi_R = \pi/2$. In particular, observing the fine structure of the distribution $\rho(m|M)$ is easier for $\phi_R = \pi/2$, as seen from Eqs. (4) - (6) of the main text. However, some correlators of the measurement outcomes can become zero for $\phi_R = \pi/2$, depending on the noise origin, and can be small for $\phi_R = 0$ [1]. This makes studying $\rho(m|M)$ for $\phi_R = \pi/4$ advantageous.

Overall, for $M = 100$ the static-limit theory is in a reasonably good agreement with the simulations of sym-metric TLSs, as seen in Fig. S3 (a) and (c). The numer-ical values of the parameter $W^{(n)}t_{\text{cyc}}$ form a geometric series and lie between $\approx 7.5 \times 10^{-3}$ and $\approx 4.7 \times 10^{-4}$. For $M = 100$ the condition $MW^{(n)}t_{\text{cyc}} \ll 1$ applies, and this is where the fine structure is most visible. Interest-ingly, for $Vt_R = 1$ the fine structure is visible even for $M = 30$, where the distribution $\rho(m|M)$ is significantly broadened by the uncertainty of the measurement out-comes. For $M = 10^3$ the distribution has a single broad peak for the both values of Vt_R. For still larger M the peak narrows down, so that ultimately the distribution
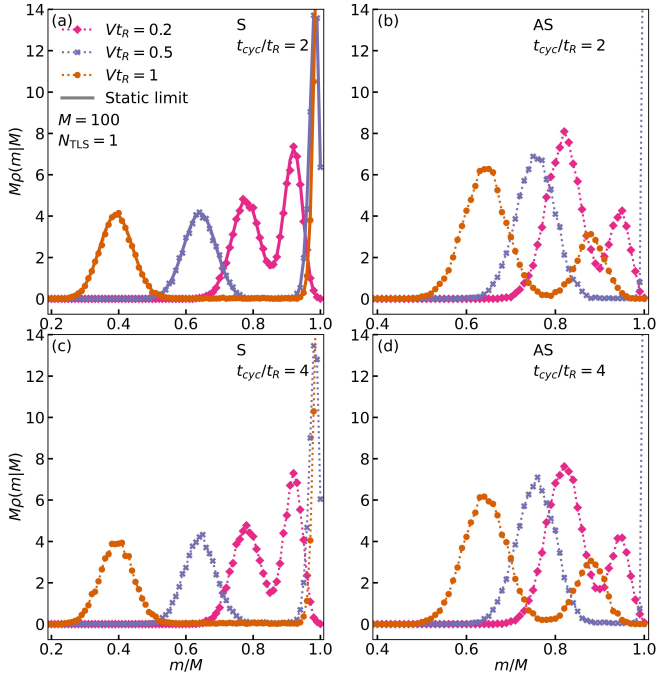
FIG. S2. Evolution of the probability distribution $\rho(m|M)$ with the varying coupling strength for a single TLS. The letters S and AS indicate that the plots refer to a symmetric or an asymmetric TLS, respectively. The scaled switching rates $W_{ij}t_R$, the measurement phase ϕ_R, and the scaled measurement periods t_{cyc}/t_R are the same as in Fig. S1. The solid theory line shows the static limit, Eq. (6) of the main text; the theory is independent of t_{cyc}.

approaches the ergodic limit.

The shape of the distribution $\rho(m|M)$ is fairly different if the TLSs are asymmetric, as seen from Fig. S3. The distribution displays fine structure, a signature of the noise from slow TLSs. Unexpectedly, as seen from panels (b) and (d), for the parameters we used, the number of well-resolved peaks is smaller when the coupling is stronger.

The qubit frequency noise from the 5 symmetric TLSs presented in Fig. S8 below is close to $1/f$ noise over almost 2 decades, which makes the analysis of the distribution $\rho(m|M)$ particularly useful in terms of identifying the noise source. The noise from 5 asymmetric TLSs has a broad $1/f$-section of the spectrum provided their coupling to the qubit is the same and the ratio of their switching rates $W_{10}^{(n)}/W_{01}^{(n)}$ is independent of n, cf. Eq. (S10) below. The shape of the distribution $\rho(m|M)$ is by far more sensitive to the features of the noise source than the power spectrum.

C. Effect of TLS asymmetry for a large number of slow TLSs

In the case of 10 TLSs with the parameters used in Fig. S4 the fine structure of $\rho(m|M)$ is not seen, simi-
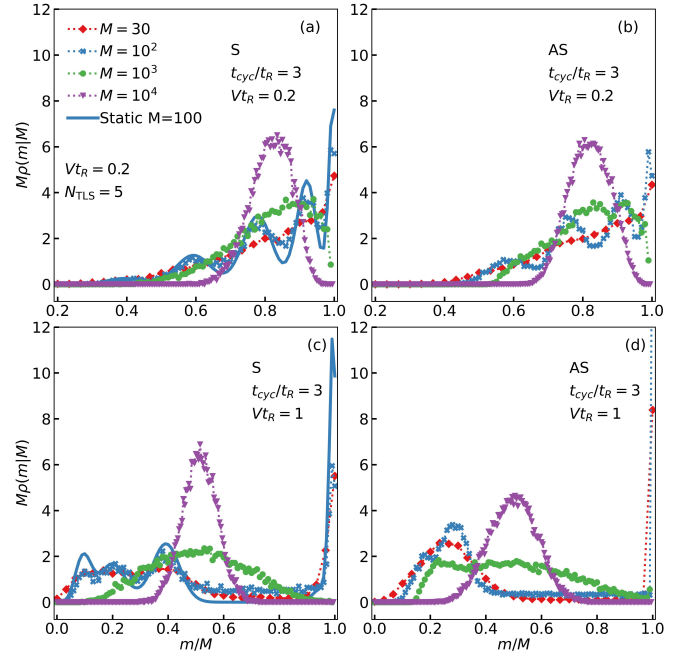
FIG. S3. Evolution of the probability distribution $\rho(m|M)$ with the varying number of measurements M for coupling to five TLSs. The letters S and AS indicate that the plots refer to symmetric or asymmetric TLSs, respectively. The measurement phase is $\phi_R = \pi/4$ and the scaled cycle period is $t_{cyc}/t_R = 3$. The number of Ramsey measurements in a sequence M and the scaled coupling parameter are indicated in the legend. For the symmetric TLSs $W^{(n)}t_R = \exp(-3n/4)$, whereas for the asymmetric TLS the scaled switching rates are $W_{10}^{(n)}\exp(-3n/4)/2$ and $W_{01}^{(n)}t_R = \exp[-3(n+1)/4]/2$ for $n = 8, 9, ..., 12$. The solid lines in panels (a) and (c) show the theory in the static approximation.

lar to the case of symmetric TLSs presented in the main text, and for the same reason, primarily: for the chosen values of the switching rates $Mt_{cyc}W^{(n)} > 1$ for several TLSs that contribute to the noise once M becomes sufficiently large, $M \gtrsim 10^2$ (we recall that M has to be large to overcome the uncertainty of the outcomes of quantum measurements). The peaks of the distribution $\rho(m|M)$ are profoundly asymmetric. Their shape displays a characteristic change with the duration of the measurement sequence Mt_{cyc} and with the effective coupling strength controlled by the Ramsey measurement duration t_R.

Somewhat unexpectedly, for the chosen parameters the evolution of the distribution for asymmetric TLSs in Fig. S4 (a) with the varying M is similar to that for symmetric TLSs in Fig. 2(b) of the main text. At the same time, in the ergodic regime, the three-time correlators for symmetric and asymmetric noises are different, although they are small in the both cases [1].
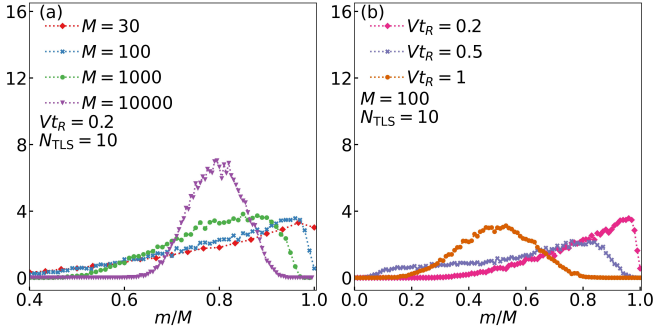
FIG. S4. Evolution of the probability distribution $\rho(m|M)$ for coupling to asymmetric TLSs. The measurement phase is $\phi_R = \pi/4$. The number of Ramsey measurements in a sequence M and the coupling parameters are indicated in the legends. The period at which the measurements are repeated within a sequence is $t_{\rm cyc} = 3t_R$. Panels (a) and (b) refer to 10 TLSs with the switching rates $W_{10}t_R = \exp(-3/4n)/2, W_{01}t_R = \exp(-3/4(n+1))/2$, where $n = 3, 4, ..., 12$.

D. Revealing asymmetry by adjusting ϕ_R

The asymmetry of TLSs can be revealed more clearly by studying the distribution $\rho(m|M)$ for $\phi_R = \pi/2$. To see this we note that the general expression for $\rho(m|M)$ in the static limit [Eq. (4) of the main text] contains a factor

$$\Theta(m, M, \ell) = \binom{M}{m} p_m[\theta(\ell)\{1 - p[\theta(\ell)]\}^{M-m}$$

For $\phi_R = \pi/2$ this factor has an important symmetry

$$\Theta(m, M, \ell) = \Theta(M - m, M, \ell) \qquad (\phi_R = \pi/2). \quad (S2)$$

Therefore, if the probability $P[\theta(\ell)]$ to have a given $\theta(\ell)$ is an even function of $\theta(\ell)$, then

$$\rho(m|M) = \rho(M - m|M) \qquad (S3)$$

The symmetry $P[\theta(\ell)] = P[-\theta(\ell)]$ holds for a Gaussian frequency noise. It holds also for symmetric TLSs. However, it does not hold for asymmetric TLSs, providing a direct means for revealing the TLSs asymmetry.

This observation should be compared with the observation that, in the ergodic limit, for $\phi_R = \pi/2$ the third centered correlator of the measurement outcomes $x_k \in \{0, 1\}$

$$\tilde{r}_3(j, k) = \left\langle \left((x_{n+k} - \langle x_{n+k} \rangle) x_{n+j} - \langle x_{n+j} \rangle)(x_n - \langle x_n \rangle) \right) \right\rangle$$

is equal to zero for Gaussian noise and for symmetric TLSs. At the same time, $\tilde{r}_3(j, k)$ is nonzero for the noise from asymmetric TLSs for this ϕ_R [1]. One can easily see that all odd-order centered correlators are equal to zero for symmetric TLSs for $\phi_R = \pi/2$. Therefore the symmetry $\rho(m|M) = \rho(M - m|M)$ applies to such TLSs beyond the static limit.
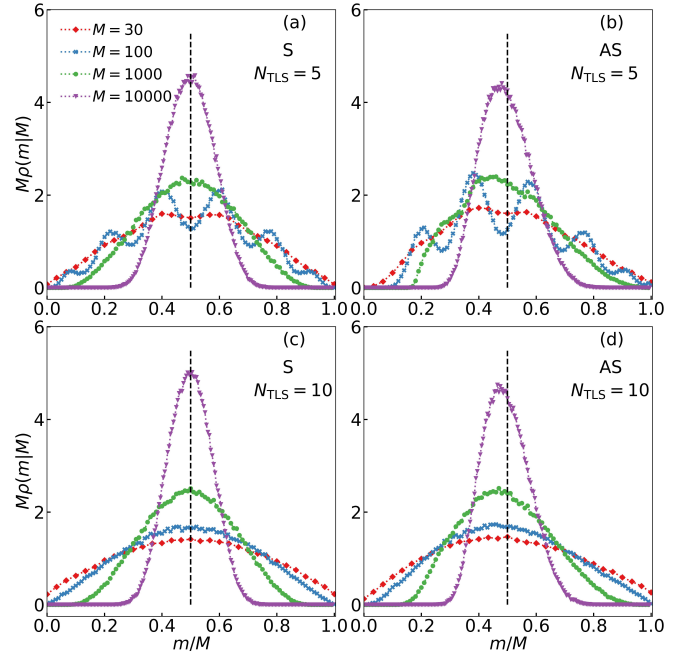

FIG. S5. Evolution of the probability distribution $\rho(m|M)$ for $\phi_R = \pi/2$. The number of Ramsey measurements in a sequence M and the number of TLSs $N_{\rm TLS}$ are indicated in the legend. The scaled coupling parameter is the same for all TLSs, $Vt_T = 0.2$, and $t_{\rm cyc} = 3t_R$. The left and right panesl refer to symmetric and asymmetric TLSs, respectively. For symmetric TLSs $W_{10}t_R = W_{01}t_R = \exp(-3n/4)/2$ whereas for asymmetric TLSs $W_{10}t_R = \exp(-3n/4)/2, W_{01}t_R = \exp[-3(n+1)/4]/2$. The values of n for 5 TLSs are $n = 8, ..., 12$, whereas for 10 TLSs they are $n = 3, ..., 12$.

Figure S5 presents the results of simulations of symmetric and asymmetric TLSs for $\phi_R = \pi/2$. A comparison of the left and right panels clearly shows that, for symmetric TLSs, the symmetry $\rho(m|M) = \rho(M - m|M)$ holds, whereas it does not hold for asymmetric TLSs. The asymmetry of asymmetric TLSs is fairly profound, both for $N_{\rm TLS} = 5$ and $N_{\rm TLS} = 10$. A comparison with Fig. S3 shows that the fine structure of $\rho(m|M)$ is also more pronounced for $\phi_R = \pi/2$ than for $\phi_R = \pi/4$, both for symmetric and asymmetric TLSs.

The possibility to use the symmetry properties of $\rho(m|M)$ adds to the value of nonergodic measurements considered in this work and shows that such measurements significantly extend the results that can be obtained using ergodic measurements. At the same time, ergodic measurements provide an important complementary information.

II. CENTERED PAIR CORRELATOR AND THE VARIANCE OF SLOW FREQUENCY NOISE

As indicated in the main text, a simple measure of closeness of $\rho(m|M)$ to the ergodic limit is the variance $\sigma_M^2 = \sum_m (m/M)^2 \rho(m|M) - r_1^2$, where $r_1 = \langle x_k \rangle \equiv$

$\sum_m (m/M)\rho(m|M)_{M\to\infty}$. A straightforward calculation shows that

$$\sigma_M^2 = M^{-1} r_1(1-r_1) + 2M^{-1} \sum_{k=1}^{M-1} \tilde{r}_2(k)[1-(k/M)],$$

$$\tilde{r}_2(k) = \langle x_n x_{n+k} \rangle - \langle x_n \rangle^2 \tag{S4}$$

Here $\tilde{r}_2(k)$ is the centered correlator of the measurement outcomes,

$$\tilde{r}_2(k) = \Big\langle (x_{n+k} - \langle x_{n+k} \rangle)(x_n - \langle x_n \rangle) \Big\rangle \tag{S5}$$

For correlated noise $\rho(m|M)$ differs from the binomial distribution and σ_M^2 is larger than its value $r_1(1-r_1)/M$ for uncorrelated noise. Still, in agreement with statistical physics, in the ergodic limit $\sigma_M^2 \propto M^{-1}$. In contrast, the static-limit value of σ_M^2 is generally much larger and scales differently with M.

A sequence of measurements approaches the ergodic limit only when its length M significantly exceeds the correlation length, i.e., $|\tilde{r}_2(M)/r_1| \ll 1$, where $r_1 \equiv \langle x_k \rangle$ is the average value of x_k. Generally, one may expect that the decay of $\tilde{r}_2(k)$ with the increasing k is an indicator of how fast the ergodicity is approached with the increasing number of measurements M.

A. Noise from TLSs

For a periodic sequence of Ramsey measurements, the centered correlator $\tilde{r}_2(k)$ was calculated both for the case where the qubit frequency noise is due to the coupling to the TLSs and for the case where the noise is Gaussian [1]. In the case of coupling to TLSs, the general expression for $\tilde{r}_2(k)$ simplifies in the limit where $V^{(n)} t_R, W^{(n)} t_R \ll 1$. One can show that, in this limit, to the leading order in the small parameters,

$$\tilde{r}_2(k) \approx \frac{1}{4} e^{-2t_R/T_2} \sin^2 \phi_R \sum_n \Big(w^{(n)} V^{(n)} t_R \Big)^2 e^{-kW^{(n)} t_{\rm cyc}},$$

$$w^{(n)} = 2(W_{01}^{(n)} W_{10}^{(n)})^{1/2}/W^{(n)}, \tag{S6}$$

whereas

$$r_1 \equiv \langle x_k \rangle \approx \frac{1}{2} + \frac{1}{2} e^{-t_R/T_2} \cos \phi_R$$
$$\times \prod_n \Big[1 - (w^{(n)} V^{(n)} t_R)^2/2 \Big]; \tag{S7}$$

the latter expression was used in the main text to give the position of the peak of $\rho(m|M)$ in the ergodic limit.

A peculiar feature of Eq. (S6) is that $\tilde{r}_2(k)$ goes to zero for $\phi_R \to 0$. For small ϕ_R we need to take into account corrections of higher-order in $V^{(n)} t_R, W^{(n)} t_R$. Using the results [1] one can show that, for $\phi_R = 0$,

$$\tilde{r}_2(k) \approx \frac{1}{4} e^{-2t_R/T_2} \Bigg\{ \sum_n \Big[w^{(n)} V^{(n)2} (\Delta W^{(n)}/W^{(n)}) t_R^2 \Big]^2$$

$$\times e^{-kW^{(n)} t_{\rm cyc}} + \sum_{m_1=1}^{N_{\rm TLS}} \sum_{m_2=1}^{m_1-1} \Big(w^{(m_1)} w^{(m_2)} V^{(m_1)} V^{(m_2)} t_R^2 \Big)^2$$

$$\times \exp[-k(W^{(m_1)} + W^{(m_2)}) t_{\rm cyc}] \Bigg\} \tag{S8}$$

where $\Delta W^{(n)} = W_{10}^{(n)} - W_{01}^{(n)}$ is the difference of the switching rates of the nth TLS. As seen from Eq. (S8), not only is $\tilde{r}_2(k)$ small for $\phi_R = 0$, but also it falls off much more rapidly with the increasing k than for $\phi_R = \mathcal{O}(1)$.

Figure S6 (a) shows $\tilde{r}_2(k)$ for the coupling to symmetric TLSs for the same parameters as in Fig. 2 of the main text. The correlator $\tilde{r}_2(k)$ is smaller for 1 TLS than for 10 TLSs for the same $\phi_R = \pi/4$. But the most significant difference is between the results for 10 TLSs for $\phi_R = \pi/4$ and $\phi_R = 0$. This difference is responsible for the difference by an order of magnitude in the values of M for which the ergodic limit is approached, as shown in the main text. It also leads to a very strong difference of the variances of the distribution shown in Fig. S6 (b). The plot of σ_M^2 here is on the linear scale, in contrast to Fig. 2 of the main text. It shows approaching the ergodic limit in more detail.
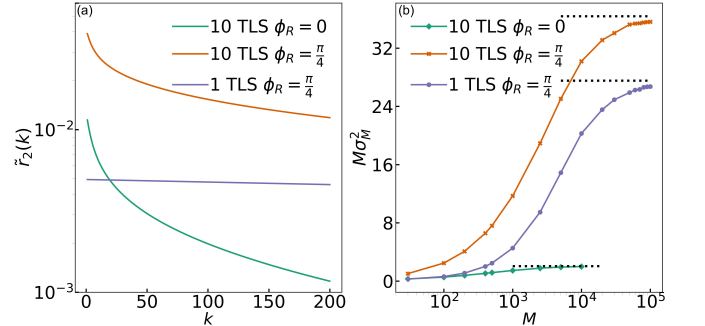

FIG. S6. Approaching the ergodic limit for noise from symmetric TLSs. Left panel: The calculated centered correlator $\tilde{r}_2(k)$ of the outcomes of qubit measurements for the quit frequency noise from TLSs. The scaled coupling is $V t_R = 0.2$. For a single symmetric TLS the scaled switching rate $W t_R = 1.2 \times 10^{-4}$. For 10 symmetric TLSs the switching rates are $W^{(n)} t_R = \exp(-3n/4)$, $n = 3, 4, \ldots, 12$. Right panel: calculated (solid lines) and simulated (dots) variance $\sigma_M^2 = \sum_m (m/M)^2 \rho(m|M) - r_1^2$ of the distribution of the outcome measurements. The dashed lines show the values of $M\sigma_M^2$ in the ergodic limit. The TLSs parameters are the same as in the left panel.

The decay of the correlator $\tilde{r}_2(k)$ with the increasing k for 10 asymmetric TLSs is shown in Fig. S7 (a). The plot refers to the same parameters as in Fig. S4. The decay is faster than for 10 symmetric TLSs, as seen from the comparison with Fig. S6 (a). Figure S7 (b) shows on the

logarithmic scale (as in the main text) how the variance of the distribution $\rho(m|M)$ approaches the ergodic limit $M \to \infty$ for the same system of 10 asymmetric TLSs. As in the case of symmetric TLSs, the variance strongly depends on the measurement phase ϕ_R. It is much smaller for $\phi_R = 0$ than for $\phi_R = \pi/4$ which, again, is a consequence of the small values and fast decay of the pair correlator $\tilde{r}_2(k)$ for $\phi_R = 0$ for slow and weakly coupled TLSs.
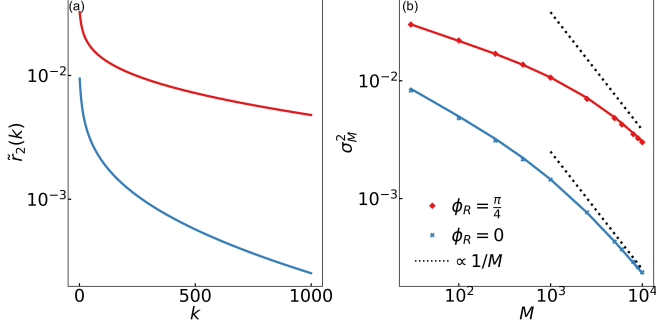

FIG. S7. Approaching the ergodic limit in the case of noise from asymmmetric TLSs. The figure refers to 10 TLSs with the same coupling parameter and the same switching rates as in Fig. S4 (a). (a): calculated centered correlator $\tilde{r}_2(k)$ of the outcomes of qubit measurements, see Eqs. (S5) and (S6), for $\phi_R = \pi/4$ (red line) and $\phi_R = 0$ (blue line). (b): calculated (solid lines) and simulated (dots) variance $\sigma_M^2 = \sum_m (m/M)^2 \rho(m|M) - r_1^2$ of the distribution of the measurement outcomes. The dashed lines show the values of σ_M^2 in the ergodic limit where $\sigma_M^2 \propto 1/M$.

B. Gaussian noise

For qubit frequency fluctuations induced by weak Gaussian noise, we have, to the leading order,

$$
\tilde{r}_2(k) \approx \frac{1}{4} e^{-2(t_R/T_2) - f_0} \left(f_k \sin^2 \phi_R + \frac{1}{2} f_k^2 \cos^2 \phi_R \right),
$$
$$
r_1 = \frac{1}{2} \left[1 + e^{-t_R/T_2} \exp(-f_0/2) \cos \phi_R \right],
$$
$$
f_k = \langle \theta_n \theta_{n+k} \rangle \qquad (S9)
$$

(we do not expand $\exp(-f_0)$, as f_0 was not very small in the simulations shown in the main text). As seen from Eq. (S9), for weak Gaussian noise $\tilde{r}_2(k)$ is much smaller for $\phi_R = 0$, similar to the case of weak noise from the TLSs.

III. NOISE POWER SPECTRUM

In the main text, the analysis of Gaussian noise was done for $1/f$-type noise with the parameters adjusted so as to make it similar to the noise from the 10 symmetric TLSs studied in the simulations with the same coupling

constants, $V^{(n)} = V$ and $w^{(n)} = 1/2$. A comparison of the noises can be done by looking at their effect on the expectation value of the measurement outcome r_1 and the power spectra.

The power spectra $S_q(\omega)$ of the noise of the qubit frequency $\delta\omega_q(t)$,

$$
S_q(\omega) = \int_{-\infty}^{\infty} dt \, e^{i\omega t} \langle \delta\omega_q(t) \delta\omega_q(0) \rangle,
$$

are shown in Fig. S8. For the noise from TLSs, the power spectrum has the form

$$
S_q^{\mathrm{TLS}}(\omega) = 2 \sum_{n=1}^{N_{\mathrm{TLS}}} (w^{(n)} V^{(n)})^2 W^{(n)} / (W^{(n)2} + \omega^2),
$$
$$(S10)$$

whereas for the Gaussian noise we studied it has the form

$$
S_q^{\mathrm{Gauss}}(\omega) = \frac{2}{\pi} D_{\mathrm{fl}} \int_{\omega_{\min}}^{\infty} \frac{dW}{W^2 + \omega^2} \qquad (S11)
$$

As seen from Fig. S8, the spectrum $S_q^{\mathrm{Gauss}}(\omega)$ is of $1/f$ type, with the low-frequency offset $\omega_{\min}$. We chose $\omega_{\min}$ to be equal to the minimal switching rate of the 10 symmetric TLSs we used in the simulations, $\omega_{\min} = \min W^{(n)}$.

It is easy to see that, for $\omega_{\min} t_R \ll 1$, the parameter f_0 that determines r_1 is

$$
f_0 \approx (D_{\mathrm{fl}} t_R^2 / \pi)(3/2 - \gamma_E + |\log(\omega_{\min} t_R)|).
$$

The value of f_0 that gives the same r_1 as the studied 10 symmetric TLSs was $f_0 \approx 0.4$. This value was used to determine the noise intensity D_{fl}.

It is seen from Fig. S8 that the spectra of the TLSs and the Gaussian noise are close at low frequencies and show $1/f$-scaling in a broad frequency range. The distributions $\rho(m|M)$ for these noises in Fig. 2 of the main text were also somewhat similar. Still there is a notable difference between the distributions, which is important for identifying the source of the noise. Interestingly, there is a comparatively small difference between the power spectra of 10 symmetric and 10 asymmetric TLSs, for the chosen parameters. In contrast, the difference between the spectra of 5 symmetric and 5 asymmetric TLSs in the inset shows is much more pronounced, although here, too the spectra are close to $1/f$ in a broad frequency ranges.

IV. INDEPENDENT MEASUREMENTS

It is instructive to compare the results on the distribution $\rho(m|M)$ with what is learned from independent Ramsey measurements separated by a time interval that largely exceeds the noise correlation time. Each such measurement has the probability

$$
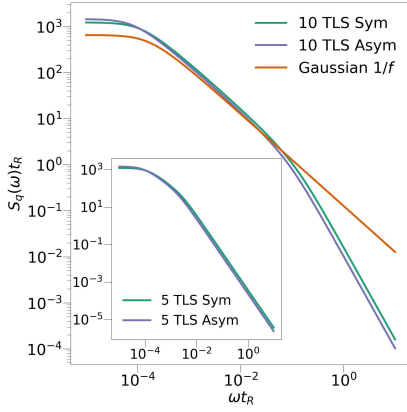p[\theta(s)] = \frac{1}{2} \left[1 + \cos\left(\theta(s) + \phi_R\right) \right]
$$

FIG. S8. Comparison of the power spectra of the $1/f$-type Gaussian noise and the noise from 10 TLSs. Plotted are the scaled spectra $S_q^{\mathrm{TLS}}(\omega)t_R$ and $S_q^{\mathrm{Gauss}}(\omega)t_R$. The spectra are given by Eqs. (S10) and (S11). The spectra for TLSs refer to the systems of 10 symmetric and 10 asymmetric TLSs with the same parameters as those in Fig. S6 and Fig. S4 (a), respectively. For the Gaussian noise we used $\omega_{\min} = \min W^{(n)}$, so that $\omega_{\min} t_R = \exp(-9) \approx 1.2 \times 10^{-4}$; $D_{\mathrm{fl}} t_R = 0.1267$. Inset: Scaled power spectra for 5 symmetric and asymmetric TLSs with the same parameters as in Fig. S3 (a) and (b).

to give "one" as an outcome. Here, the values of the phase $\theta(s)$ are random, they are enumerated by $s = 1, 2, ..., M$.

As the measurements are repeated, we may expect to obtain a binomial distribution of the outcomes. For the generating function of the distribution of the outcomes x_k of independent individual measurements we have

$$\left\langle \exp\left[(t/M)\sum_{k=1}^{M} x_k\right]\right\rangle = \prod_k \left\langle \exp\left(tx_k/M\right)\right\rangle$$
$$= \{1 + r_1[\exp(t/M) - 1]\}^M, \qquad \text{(S12)}$$

where $r_1 \equiv \langle x_k \rangle$ is the expectation value of x_k.

At the same time, for the binomial distribution $\rho_{\mathrm{binom}}(m|M)$, Eq. (3) of the main text, we have $\langle \exp(tm/M)\rangle = \{1 + r_1[\exp(t/M) - 1]\}^M$. This expression coincides with the generating function (S12). This is to be expected, since making consecutive measurements separated by the time longer than the noise correlation time is essentially equivalent to making a long series of experiments with the total length largely exceeding the correlation time.

For completeness, we demonstrate in Fig. S9 that the presence of qubit frequency fluctuations with a short correlation time along with the noise from slow TLSs

V. EFFECT OF STATE PREPARATION, MEASUREMENT ERRORS AND A BROAD-BAND FREQUENCY NOISE

The standard expression for the probability to have the outcome of a kth measurement $x_k = 1$, Eq. (2) of the main text, refers to the case where the qubit is initially prepared in state $|0\rangle$. The preparation relies on resetting the qubit to $|0\rangle$ by resonantly coupling it to a dissipative reservoir at temperature much smaller than the qubit energy spacing in the appropriate units. For example, the qubit can be coupled to a fast decaying radiation mode. Such preparation breaks the coherence of the qubit, but the presence of stray excitations in the reservoir may result in exciting the qubit to state $|1\rangle$. The initial qubit state is then described by the density matrix

$$\rho_q(0) = (1 - \varepsilon_{\mathrm{reset}})|0\rangle\langle 0| + \varepsilon_{\mathrm{reset}}|1\rangle\langle 1|.$$

The gate operations leading to the Ramsey rotations of the qubit can also have an error. The simplest model is where both rotations have the same error ε_g, so that the corresponding unitary operation is $\exp\{-i[(\pi/4) + \varepsilon_g]\sigma_y\}$.

We can also take into account the possibility of a readout error, that is, the possibility that, when in a kth measurement the qubit is in state $|1\rangle$, the probability to read out $x_k = 1$ is $1 - \varepsilon_{01}$, whereas when the qubit is in state $|0\rangle$ the probability to read out $x_k = 1$ is ε_{10}. To the lowest order of the perturbation theory, these errors lead to a correction of the expression for $p(\theta)$,

$$p(\theta) \approx \frac{1}{2}\left(1 - 4\varepsilon_g^2 - \varepsilon_{01} + \varepsilon_{10}\right)$$
$$+ \frac{1}{2}\left[1 - (2\varepsilon_{\mathrm{reset}} + \varepsilon_{01} + \varepsilon_{10} + 4\varepsilon_g^2)\right]\cos(\phi_R + \theta) \quad \text{(S13)}$$

where we have disregarded the factor $\exp(-t_R/T_2)$.

A less realistic error model is that the initial state is $[|0\rangle + \varepsilon_0|1\rangle]/(1 + \varepsilon_0^2)^{1/2}$ and that the first Ramsey gate is $\exp[-i(\pi/4 + \varepsilon_{1g})\sigma_y]$ and the second Ramsey gate is $\exp[-i(\pi/4 + \varepsilon_{2g})\sigma_y]$ and that all errors are independent from each other, so that the cross-terms like $\varepsilon_0\varepsilon_{1g}$ can be disregarded. In this model

$$p(\theta) = \{1 + \cos(\theta + \phi_R)[1 - 2(\varepsilon_0^2 + \varepsilon_{1g}^2 + \varepsilon_{2g}^2)]\}/2.$$

The decrease of the term $\propto \cos(\phi_R + \theta)$ indicates that the errors make the measurements less sensitive to the phase. However, in the high-end quantum computers implemented nowadays all these errors are very small.

does not lead to disappearance of the fine structure of $\rho(m|M)$. Panel (b) shows the simulated $\rho(m|M)$ for random values of θ that are uncorrelated between suc-
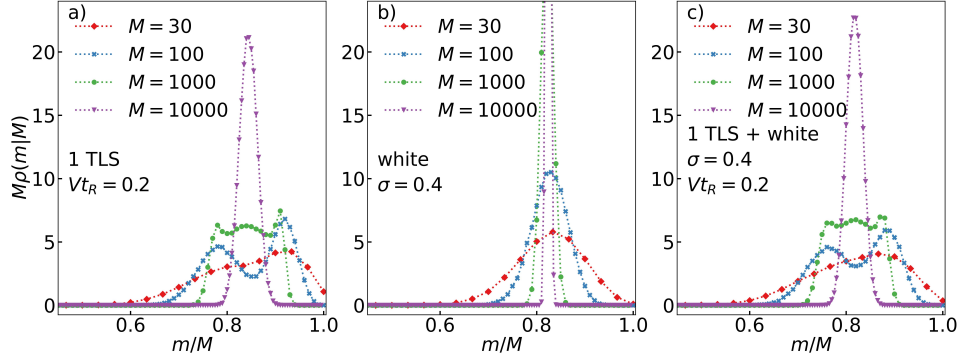
FIG. S9. Effect of an extra short-time-correlated frequency noise on the visibility of the fine structure. (a) The distribution $\rho(m|M)$ for a single symmetric TLS with $Wt_R = 1.2 \times 10^{-4}$. (b) The distribution $\rho(m|M)$ for white Gaussian noise in the phase θ with standard deviation $\sigma = 0.4$. (c) The distribution $\rho(m|M)$ in the presence of the both noises in (a) and (b).

cessive measurements and have Gaussian distribution $w_\theta = (2\pi\sigma^2)^{-1/2}\exp(-\theta^2/2\sigma^2)$. This model describes white noise in θ that results from a Gaussian noise in the qubit frequency $\delta\omega_q(t)$ with the correlation time smaller than the time separating the measurements t_{cyc}. In this case $\rho(m|M)$ is just the standard binomial distribution.

In Fig. S9 (c) we show $\rho(m|M)$ in the case where fluctuations of $\delta\omega_q(t)$ come from both white noise in θ and the noise from a single slow symmetric TLS. A comparison of the panels (a) and (c) demonstrates that the characteristic fine structure of $\rho(m|M)$ remains well resolved even though the intensity of the white noise is not small.

[1] F. Wudarski, Y. Zhang, A. N. Korotkov, A. Petukhov, and M. Dykman, Characterizing Low-Frequency Qubit Noise, Phys. Rev. Appl. **19**, 064066 (2023).